Plasma Dynamics with Second and Third Harmonic ECRH on TCV

L Porte[1], S Coda[1], S Alberti[1], G Arnoux[2], P Blanchard[1], A Bortolon[1], A Fasoli[1], TP Goodman[1], Y Klimanov[1], Y Martin[1], M Maslov[1], A Scarabosio[1] and H Weisen[1]

[1] Ecole Polytechnique Fédérale de Lausanne (EPFL)
Centre de Recherches en Physique des Plasmas
Association Euratom-Confédération Suisse
CH-1015 Lausanne, Switzerland
[2] present address Association EURATOM-CEA, CEA/DSM/DRFC,
CEA-Cadarache, St. Paul lez Durance, France

E-mail: laurie.porte@epfl.ch

Abstract. Intense electron cyclotron resonance heating (ECRH) and electron cyclotron current drive (ECCD) are employed on the Tokamak à Configuration Variable (TCV) both in second- and third-harmonic X-mode (X2 and X3). The plasma behaviour under such conditions is driven largely by the electron dynamics, motivating extensive studies of the heating and relaxation phenomena governing both the thermal and suprathermal electron populations. In particular, the dynamics of suprathermal electrons is intimately tied to the physics of X2 ECCD. ECRH is also a useful tool for manipulating the electron distribution function in both physical and velocity space. Fundamental studies of the energetic electron dynamics have been performed using periodic, low-duty-cycle bursts of ECRH, with negligible average power injection, and with electron cyclotron emission (ECE). The characteristic times of the dynamical evolution are clearly revealed. Suprathermal electrons have also been shown to affect the absorption of X3 radiation. Thermal electrons play a crucial role in high-density plasmas where indirect ion heating can be achieved through ion-electron collisions. In recent experiments $\approx 1.35\ MW$ of vertically launched X3 ECRH was coupled to a diverted ELMy H-mode plasma. In cases where $\geq 1.1\ MW$ of ECRH power was coupled, the discharge was able to transition into a quasi-stationary n ELM-free H-mode regime. These H-modes operated at $\beta_N \approx 2$, $\overline{n_e}/n_G \approx 0.25$ and had high energy confinement, $H_{IPB98(y,2)}$ up to ≈ 1.6. Despite being purely electron heated and having no net particle source these discharges maintained peaked electron density profiles ($n_{e,o}/<n_e> \approx 1.6$). They also exhibited spontaneous toroidal momentum production in the co-current direction. The momentum production is due to a transport process as there is no external momentum input. This process supports little or no radial gradient of the toroidal velocity.

PACS numbers: 52.55.Fa, 52.50.Gj, 52.25.Sw

1. Introduction

Intense electron cyclotron resonance heating (ECRH) is employed on the TCV both in second- and third-harmonic X-mode (X2 and X3) [1]. Suprathermal electrons play a significant role in ECRH physics and in particular, their dynamics is intimately tied to the physics of X2 current drive (ECCD) [2-3]. The absorption of third-harmonic X-mode (X3) radiation can be enhanced by the presence of these high-energy electrons, which can also be generated by the X3 wave itself [4-6]. Suprathermal electrons are also generated by the strong electric fields created by the magnetic reconnection events accompanying sawtooth crashes [7], a subject not discussed in this paper.

Electrons play an important role in high density plasmas where indirect ion heating can be achieved though ion-electron collisions. This aspect of electron dynamics is of fundamental importance to fusion relevant machines where a significant fraction of ion heating is expected through the $\alpha \rightarrow$ electron $\rightarrow$ ion channel. Access to higher density also enables the experimental study of electron heating in H-mode plasma where means are still being sought to mitigate the effects of core impurity accumulation and first wall erosion caused by ELMs.

These facets of plasma dynamics can be addressed on TCV using the X3 system, which allows access to plasma at density greatly exceeding the X2 cut-off, and particularly in H-mode [10]. The X3 beams are launched vertically from the top of the vessel, parallel to the resonant surface, in order to maximize first-pass absorption of the inherently weakly damped waves [5]. X2, with its short wavelength and excellent deposition localization, is an ideal tool for direct manipulation of the electron distribution function. Fully non-inductively sustained electron internal transport barriers in TCV [11] exemplify this, combining velocity-space control (current drive) with real-space control (shear reversal).

In this paper we will describe two recent sets of experiments, the first set aimed at studying the dynamics of the electron distribution function in the presence of X2 ECCD and X3 ECRH and the second set to heat H-mode plasma, using X3.

2. TCV and the ECRH system

2.1. The Tokamak à Configuration Variable (TCV)

TCV has a major radius of 0.88 m and a minor radius of 0.25 m. Operation is generally conducted with a toroidal magnetic field, B_ϕ, $\leq$ 1.54 T and a plasma current, I_p, $<$ 1 MA with an elongation, κ, $<$ 2.7. The plasma facing wall is made entirely of graphite and is routinely boronised. TCV was designed to allow the study of plasma with extreme shaping and is equipped with a powerful and versatile ECRH/ECCD system for additional heating.

2.2. The Electron Cyclotron Resonance Heating And Current Drive System on TCV

TCV is equipped with 6 gyrotrons that operate at 82.7 GHz for X2 heating and current drive [12] and three gyrotrons that operate at 118 GHz providing X3 heating [13].

Each X2 gyrotron delivers 450 kW for up to 2 sec from the low-field side (LFS) of the tokamak, each through its own launcher that is furnished with real-time control of the launch angle. Cut-off and refraction limit the range of density over which the X2 system can be used to $n_{max} \approx 4.2 \times 10^{19}\ m^{-3}$.

The X3 system has three 470 kW gyrotrons, also with 2 sec pulse length. Absorption of the X3 wave is weak, lower than X2 absortion by a factor $(k_B T_e)/(m_e c^2)$, so a vertical launch system is employed to maximise the optical depth. In this geometry the X3 power is launched with wavevector perpendicular to the magnetic field and therefore there is no net current drive. Each gyrotron has a dedicated transmission line. The three transmission lines are directed toward a single plasma facing mirror the radial position (R_L) of which can be adjusted between shots. Its poloidal launch angle (θ_L) may be swept during a discharge. X3 operation is limited to density below $11.0 \times 10^{19}\ m^{-3}$.

3. Plasma Dynamics

3.1. Suprathermal Electron Dynamics

In the very high power density conditions of X2 ECCD experiments in TCV, the dynamics of the high-energy electrons accelerated by the EC waves is unusually complex, as rf diffusion, collisional slowing-down and pitch-angle scattering in velocity space and cross-field transport in physical space all operate on comparable characteristic time scales [3]. In particular, radial transport has the effect of regulating the quasi-linear enhancement of ECCD efficiency and of broadening the driven current profile. The fundamental role played by suprathermal electrons in some of the key scenarios developed and explored in TCV has motivated a series of dedicated studies of the energetic electron dynamics under controlled conditions.

These studies employed periodic, low-duty-cycle bursts of ECRH (X2 ECCD or X3) in conjunction with high-field-side (HFS) electron cyclotron emission measurements, which were coherently averaged over a stationary period comprising several tens of pulses [8]. The low average injected power ensured that the plasma was not significantly perturbed. The aim of this work was to follow the signal dynamics after power shut-off and identify the characteristic relaxation times and the full dynamical characteristics of the system.

The study was articulated in a series of systematic scans of plasma and ECRH parameters. The time-to-peak is an appropriate simple parameter to illustrate the dynamics, as it depends on both the characteristic transport time and the slowing-down time. The effect of radial transport was clearly seen in the time-to-peak plotted as a function of frequency, see Fig. 1a, for a case with centrally applied ECCD pulses and

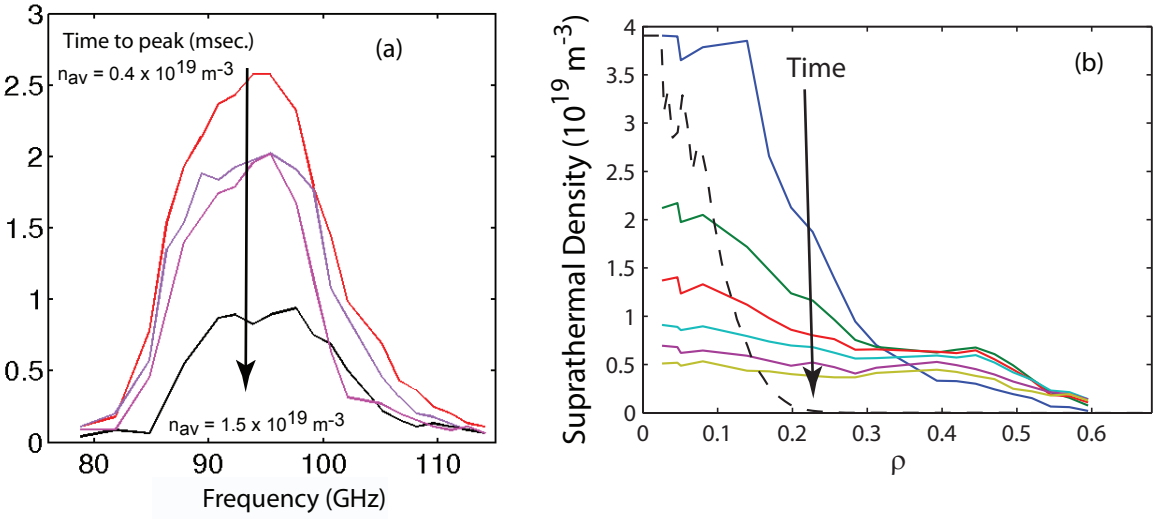

Figure 1. : (a) The time-to-peak of HFS ECE from pulsed ECCD, as a function of RF frequency and line-averaged plasma density (0.4, 0.8, 1.1 and 1.5 $\times$ $10^{19}m^{-3}$). (b) reconstructed suprathermal density profiles at 0, 0.1, 0.2, 0.3, 0.4 and 0.5 msec after the ECCD turn off; the time order is as indicated by the arrow, The dashed curve is the power deposition profile calculated by ray tracing, in arbitrary units. Average injected power 40 kW, plasma current 230 kA, line average density 1.5 $\times$ $10^{19}m^{-3}$.

the ECE horizontal sightline lying on the plasma mid-plane. The rise at low frequency corresponded to X2 emission from locations increasingly off-axis on the HFS, whereas the rollover at high frequency was attributed to X3 emission from the LFS moving towards the center. The strong reduction of the time-to-peak with increasing density reflects primarily the corresponding reduction in the slowing-down time [8].

Resolving both the energy and the emission location in HFS ECE measurements is impossible. However, quantitative insight was obtained by adopting a simple bi-Maxwellian approximation for the electron distribution function. Employing the further assumption, verifiable a posteriori, that the relatively tenuous suprathermal component was optically thin, the suprathermal density profile was recovered from the ECE data [9]. As shown in Fig. 1b, the spatial broadening caused by radial transport, as well as the overall temporal decay of the population caused by collisional momentum destruction, were clearly visualized through this technique. A simple diffusive model was applied to this case, allowing a representative diffusivity and decay time to be derived by a fit to the data, as shown in Fig. 2. The resulting diffusivity (12.6 m^2s^{-1}) was well above the typical values cited in the literature; this result must, however, be seen as merely illustrative of the transport process at play, owing to the simplicity of the model. More extensive semi-analytical or Fokker-Planck modelling will be required to further constrain the system dynamics. It is worth noting that in a study of suprathermal electrons accelerated (to $10-15$ keV) by the electric fields generated by sawtooth crashes in TCV, the radial diffusivity was been estimated to on the order of $25m^2s^{-1}$[10].

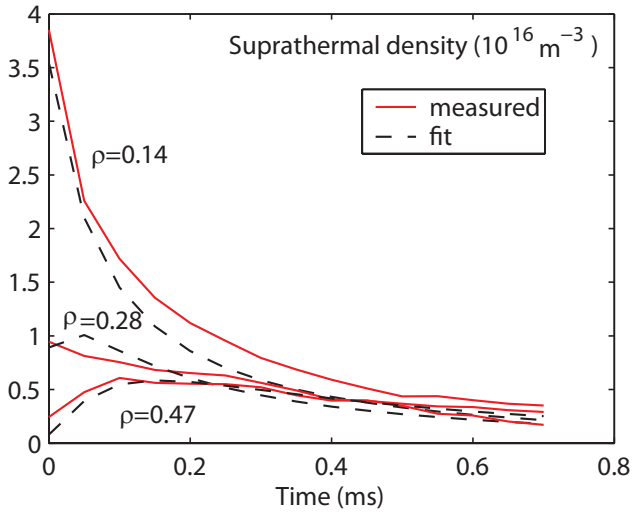

Figure 2. : measured and fitted time traces of the suprathermal density at three different radial locations, for the case of Fig. 1b. The fit is based on a cylindrical diffusive model with diffusivity $D = 12.6\ m^2 s^{-1}$ and decay time $\tau = 1.5\ ms$.

The suprathermal electron population generated by X2 ECCD is also believed to be responsible for the observed enhanced absorption of laterally-launched X3 waves with respect to calculations based on a Maxwellian population [4]. Recent work has demonstrated that a simplified ad-hoc electron distribution function model (in this case a combination of two truncated Maxwellians) can succeed in reproducing all the salient measurements, namely the power absorption, the ECE radiative temperature and the hard X-ray emissivity [10].

In another set of experiments the energetic electron dynamics was investigated by using X3 to couple to electrons in the tail of the thermal electron distribution [5, 8]. In this experiment the X3 power was modulated (on/off) with a duty cycle of 50% allowing the absorbed X3 power to be measured using a Diamagnetic Loop (DML). The average X3 power was 650 kW. The X3 mirror angle was swept, in steps of 0.5 deg with a 200 $msec$ pause at each step, form the low-field-side to the high-field-side (LH) and from the high-field-side to the low-field-side(HL), in two separate discharges. In this way the absorbed X3 power could be determined as a function of launcher angle and as a function of the direction of the launcher sweep. The supra-thermal electron dynamics were compared with the bulk electron dynamics by comparing measurements of HFS-ECE (radiative temperature, $T_{e,rad}$) and Thomson scattering (bulk temperature, $T_{e,th}$).

In figure 3 the dynamics of the two scenarios, LH and HL, are compared. The absorbed X3 fraction for LH is shown in (a) while that for HL is shown in (b). In both cases the maximum absorbed power was $\approx 65\%$ but the curves were not symmetric: the optimal angles are different: $\theta^{LH}_{l,opt} \approx 45.9°$ for LH and $\theta^{HL}_{l,opt} \approx 46.3°$ for HL. The asymmetry can be understood qualitatively as follows: in the HL scenario power is

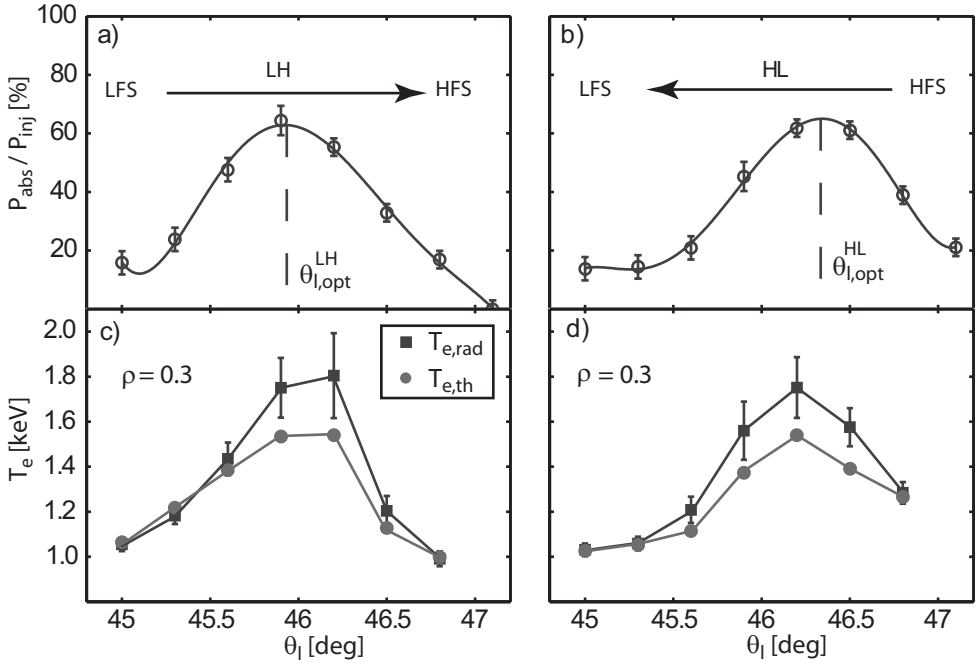

Figure 3. : The absorbed X3 fraction, as measured using a DML, as a function of X3 launcher angle, θ_l, for sweeps moving from LFS to HFS (a) and vice-versa (b). The temporal average of $T_{e,th}$ and $T_{e,rad}$ (from $\rho = 0.3$) measured as a function of θ_l during the X3 launcher sweep. LFS to HFS (c) and HFS to LFS (d).

coupled to suprathermal electrons first, and from these to the bulk electrons through collisional transfer, resulting in optimal power absorption before the beam reaches the nominal (cold) resonance; in the LH case, by contrast, coupling with the thermal electrons occurs first. (Note that the suprathermal electrons are generated by the X3 wave itself.) The nonlinearities in the system can then make the two paths asymmetric, as evidenced e.g. by the different bulk temperatures at the same angle of 46.5 deg (1.4 keV in the HL case and 1.1 keV in the LH case).

This preliminary study revealed that suprathermal electrons can play a significant role in X3 bulk heating. The observation that the X3 wave can alter the electron energy distribution function which then in turn alters the X3 bulk heating has yet to be reproduced in Fokker-Planck simulations. A deeper study, using X3 power blips akin to those used in X2, will be used in the future to study the suprathermal electron relaxation dynamics.

4. X3 Heating of ELMy H-mode on TCV

4.1. The ELMy Ohmic H-mode Target

One of the main goals of TCV is to study plasma at or near the β-limit. To do this requires high plasma pressure which can be achieved by additionally heating H-mode.

In most H-mode scenarios ions are directly heated using Neutral Beam Injection

(NBI), Ion Cyclotron Resonance Heating (ICRH) or a combination of both. Electrons are usually heated through electron-ion collisions. TCV is in the unique position of being able to achieve H-mode and directly heat electrons using X3 ECRH leaving the ions to be heated by ion-electron collisions: a scenario that mimics the burning plasma scenario where ions are heated through the $\alpha \rightarrow e^- \rightarrow ion$ channel.

The goal of achieving high performance H-mode and the physics interest of exploring H-mode with pure electron heating motivated a series of experiments where a pre-existing ohmic ELMy H-mode was heated using X3. This target scenario lends itself to X3 heating because of its inherently high, compared to L-mode, temperature ($T_e \approx 1\ keV$; $T_i \approx 550\ eV$) and high, compared to L-mode, energy confinement ($\tau_E \approx 45\ msec.$) both of which help increase the X3 absorption.

The target was a single null diverted discharge with the ion-$\vec{\nabla}|\vec{B}|$ direction away from the X-point. The plasma current was in the range $390\ kA \leq I_p \leq 420\ kA$ while the plasma density was typically $n_e \approx 7 \times 10^{19}\ m^{-3}$, close to the optimum for X3 heating and $\approx 25\%$ of the Greenwald density. $B_{tor} = 1.45\ T$, $\kappa_{95} = 1.65$ and $\delta_{95} = 0.36$ while $d_{inner} = 3\ cm$ and $q_{95} \approx 2.4$. The stored energy $W_{dia} = 20\ kJ$ and the energy loss per ELM was $\delta W_{dia,ELM}/W_{dia} \approx 4\%$. The energy confinement time in the ohmic phase of these discharges was well described by the IPB98(y,2) [14] scaling and it is with reference to this scaling that H-factors are calculated in this paper.

Detailed experimental studies of third harmonic absorption have recently been performed on TCV and details are to be found in [5, 6, 15]. The salient point for vertically launched X3 heating is the linear dependence of the absorption on electron temperature. With the electron density near the optimum for X3 heating ($\approx 7 \times 10^{19}\ m^{-3}$), then once T_e rises above $2\ keV$ the single pass X3 absorption exceeds $\approx 80\%$ and substantial heating is possible.

It has been shown [15] that in H-mode, ray-tracing estimates of X3 power absorption, by TORAY-GA [16], are in good agreement with measurements made using a DML [17] indicating that the electron distribution functions were thermal. All estimates of X3 absorbed power, presented in this paper, have been obtained using TORAY-GA.

4.2. Characteristics of X3 Absorption in H-mode Plasma

Figure 4 shows the temporal evolution of the X3 coupled power in a typical X3 heated ELMy H-mode case. Initially, the X3 absorption was low ($\approx 40\%$) but quickly increased to $\approx 70\%$ ($1.05\ MW$ of coupled X3 power) as T_e (not shown) increased from $1.0\ keV$ to $\approx 1.8\ keV$. At the same time the ohmic power fell from $\approx 500\ kW$ to $\approx 300\ kW$. The total heating power therefore increased from $500\ kW$ to $\approx 1.35\ MW$. The X3 heating power was maintained at this high level despite the ELMs which can potentially refract power away from the resonance.

According to TORAY-GA, the power deposition region lay in the region $0.05 \geq \rho \geq 0.9$. The RF beam was projected toward the high field side of the resonance to benefit from absorption on the relativistically broadened resonance.

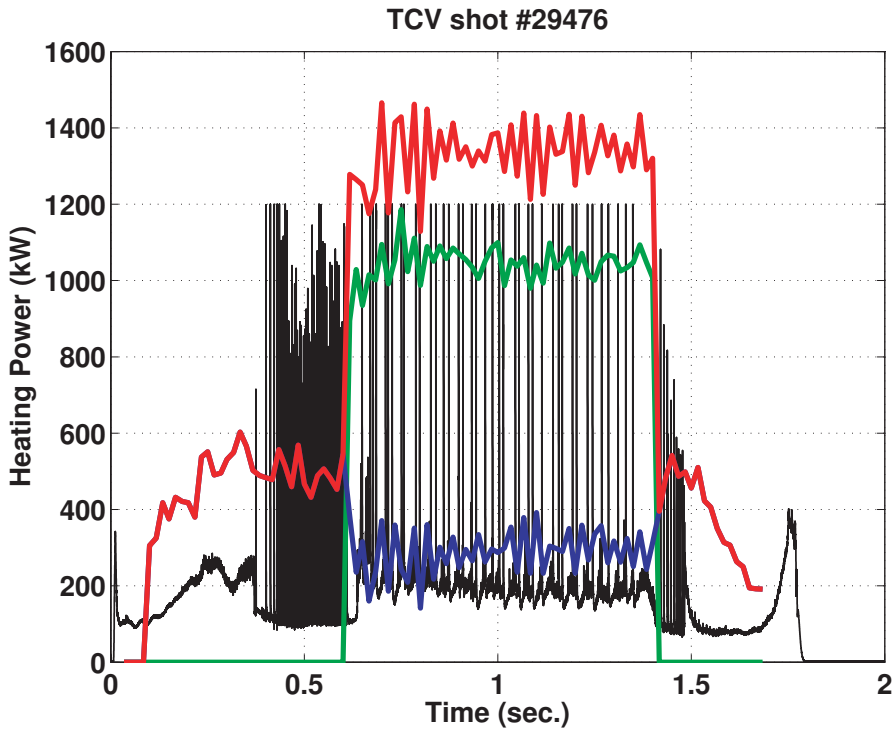

Figure 4. Temporal evolution of the D_α emission (black; arbitrary units), ohmic heating power (P_Ω; blue), X3 coupled power ($P_{X3,coupled}$; green) and the total heating power ($P_{total} = P_\Omega + P_{X3,coupled}$; red) for shot 29476, a typical X3 heated H-mode. The X3 heating phase lasts from 0.6 *sec.* until 1.4 *sec.*

The mirror-angular region over which good X3 absorption takes place is typically $\approx 0.5°$ for an electron temperature of 1 keV. However, as the plasma heats this angular range increases, due to the relativistic dependence of the electron mass on energy. At 3 keV the angular width is $\approx 2°$ and the absorption is much less sensitive to density changes making it possible to compensate for refraction of the RF beam by adjustment of the mirror angle a priori.

4.3. Quasi-Stationary ELM-free H-Mode Phase

4.3.1. General Characteristics Using three X3 gyrotrons the available power at the plasma was ≈ 1.45 MW. When the absorbed fraction greatly exceeded the L- to H-mode transition power (≈ 500 kW) a quasi-stationary, ELM-free H-mode (QSEFHM) regime could be obtained.

The QSEFHM regime was characterised by elevated D_α light emission compared to the baseline ohmic ELMy H-mode, approximately constant $\overline{n_e}$, constant W_{dia}, high β_{tor} and high τ_E. An example of this remarkable regime is shown in Figure 5. An ohmic ELMy H-mode was heated using X3. The X3 heating period started at 0.6sec. The discharge entered a Type-I ELMy phase that lasted for ≈ 200 $msec$ at which point it transitioned into a QSEFHM phase. The QSEFHM phase lasted, uninterrupted, until

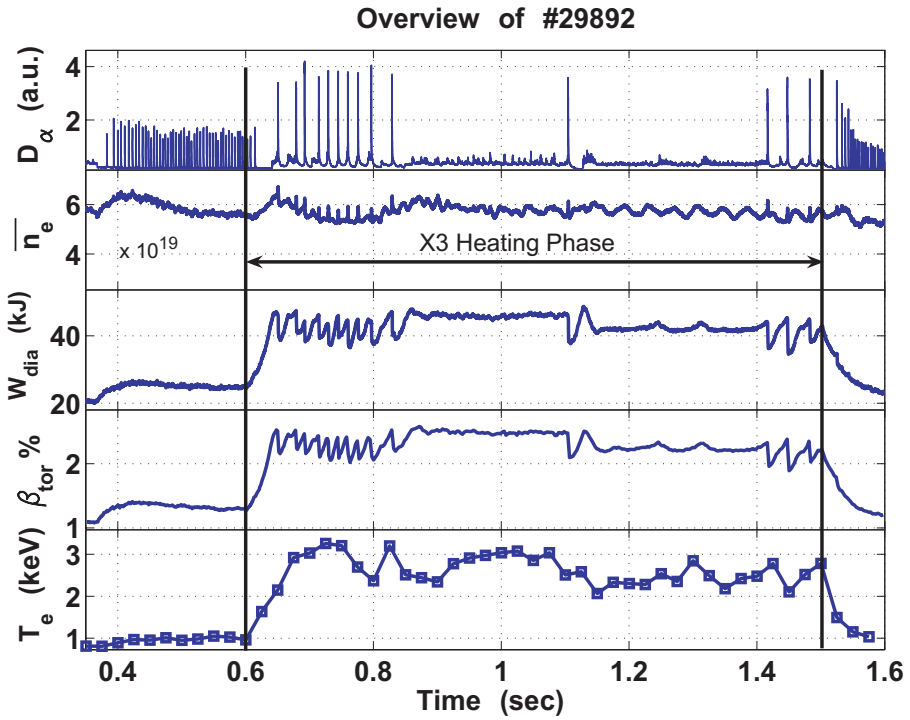

Figure 5. Overview of TCV shot 29475. From top to bottom, the D_α light, $\overline{n_e}$, the stored energy, β_{tor} and electron temperature. This discharge was an ELMy H-mode target heated with $\approx$ 1.4 MW of total heating power in the period 0.6 *sec.* until 1.4 *sec.*.

1.1sec ($\approx$ 10 confinement times) and was terminated by a large ELM. Subsequently the discharge entered a brief ELM-free H-mode phase before entering a second QSEFHM period that continued until 1.4sec.

The electron pressure profiles were very similar in the ohmic H-mode phase, the Type-I ELMy phase and the QSEFHM phase (n.b. the high resolution Thomson scattering diagnostic was not available for this campaign so changes in the extreme edge, $\rho > 0.9$, pressure profile could not be resolved). Figure 6 compares electron temperature, electron density and incremental X3 absorption profiles from a discharge in which both the large-ELM regime and the quasi-stationary ELM-free H-mode regime were observed. There are no significant differences between all the profiles during the three phases so formation of the QSEFHM cannot be attributed to a change in X3 power deposition.

The measured β_{tor} was $\approx$ 2.5% (c.f. $\beta_{limit,ideal} \approx 3.5\%$) and the confinement time was $\approx$ 30 $msec$ ($H_{IPB98(y,2)} \approx 1.4$), for the QSEFHM regime, at full heating power. Values of $H_{IPB98(y,2)} \approx 1.6$ have been transiently achieved.

In the ohmic phase the density peaking factor, $n_{e,o}/<n_e>$, was $\approx$ 1.68 while in both the Type-I ELMy phase and the ELM-free quasi-stationary phase it was reduced to between 1.5 and 1.6. Numerical simulations, using the KN1D code [18] indicated

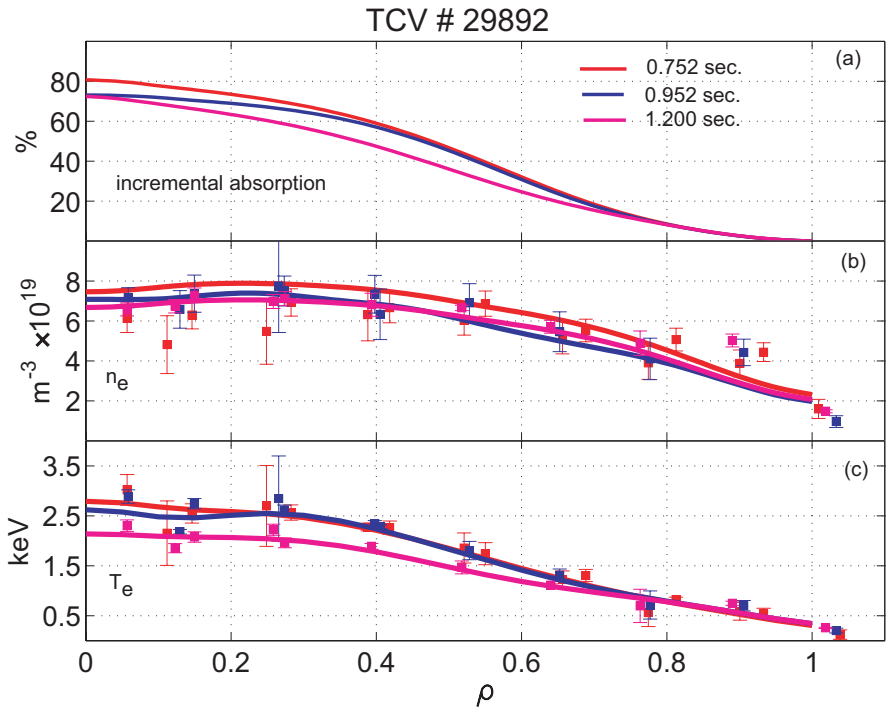

Figure 6. Profiles of (a) incremental X3 absorption, (b) electron density and (c) electron temperature for three different phases of TCV shot 29892.

that edge fueling played no role in maintaining the density peaking in these discharges. The low loop voltage in these discharges also suggested that the Ware pinch was not involved in maintaining the density peaking. An anomalous particle pinch mechanism must be at work [19, 20].

Measurements of soft X-ray emission revealed no sign of impurity accumulation during the quasi-stationary ELM-free phase; $Z_{eff} \approx 2.5$ in the ohmic phase and increased to ≈ 3 in the X3 phase. The radiated power (P_{rad}) was $\approx 300\ kW$ and did not increase during the quasi-stationary phase.

4.3.2. MHD The quasi-stationary ELM-free phase of TCV H-mode discharges exhibited core MHD activity. They were typically dominated either by m/n = 1/1 modes (sawtooth precursors) that were present throughout the discharges or by m/n = 4/3 tearing modes that were associated with reduced energy confinement compared to the m/n = 1/1 dominated phases. The fluctuations observed on the D_α light during the QSEFHM phase were not ELMs. Rather they were strongly correlated with the sawteeth.

To date no MHD signature similar to the so-called Edge Harmonic Oscillation (EHO) [26] has been measured on TCV.

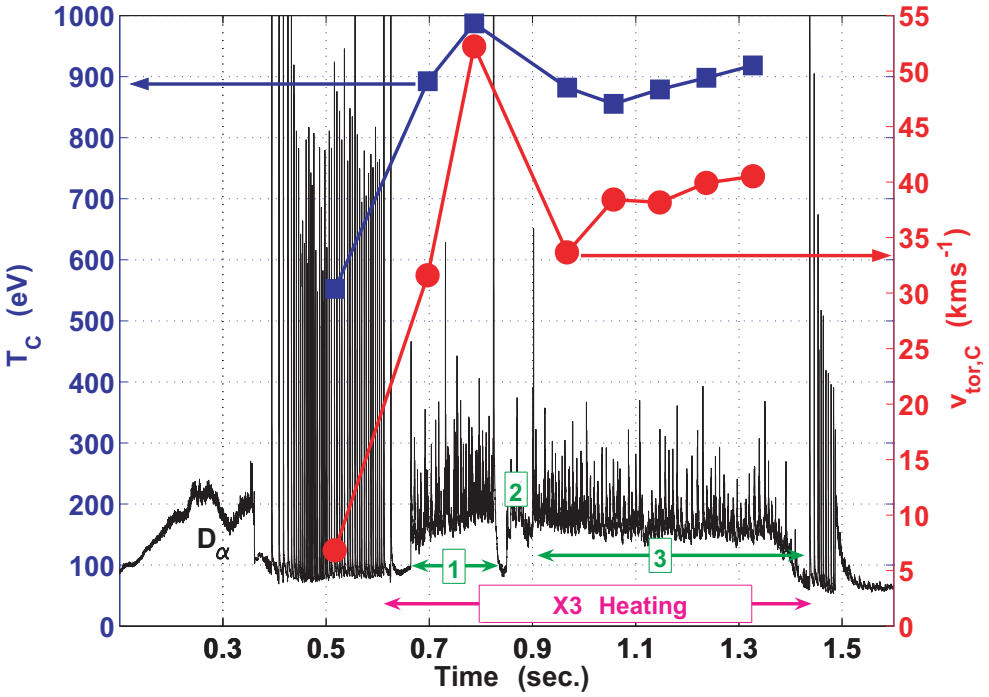

Figure 7. D_α light with the temporal evolution of the carbon ion temperature and carbon ion toroidal rotation velocity at $\rho \approx 0.6$ for shot number 29475. Shown also are the X3 heating phase (pink) and the three quasi-stationary H-mode phases (green) labelled 1, 2 and 3.

4.3.3. Ion Behaviour During the quiescent H-mode phase it was possible to measure the carbon ion toroidal rotation, $v_{tor,C}$, and carbon ion temperature profiles, T_C. These measurements were made using the TCV Charge Exchange Recombination Spectroscopy (CXRS) diagnostic [21]. Due to the line of sight used by the CXRS system it was not possible to obtain measurements of T_C and $v_{tor,C}$ inside $\rho \approx 0.6$.

Figure 7 shows the temporal evolution of the D_α recycling light, the T_C and $v_{tor,C}$, both at $\rho \approx 0.6$, for shot 29475. The X3 heating phase lasted from 0.6 *sec* to 1.4 *sec*. For the first time significant ion heating has been measured on TCV. At mid-radius the ion temperature increased from $\approx$ 500 eV to $\approx$ 1 keV. At the same time the carbon ion toroidal rotation speed was measured to increase significantly; this is despite the fact that the X3 heating produces no net momentum. Neutral Particle Analyser measurements show that the ion distribution function remained thermal during X3 heating.

In this discharge there were three QSEFHM phases. The first (1), in the period 0.68 *sec*. to 0.83 *sec*., was dominated by a m/n=1/1 mode while the second (2), in the period 0.84 *sec*. to 0.9 *sec*. was dominated by an m/n=4/3 mode. The m/n = 4/3 mode degraded the plasma performance and both the T_C and the $v_{tor,C}$ fell. In the third (3) quasi-stationary ELM free phase in the period 00.9 *sec*. to 1.37 *sec*. the discharge was

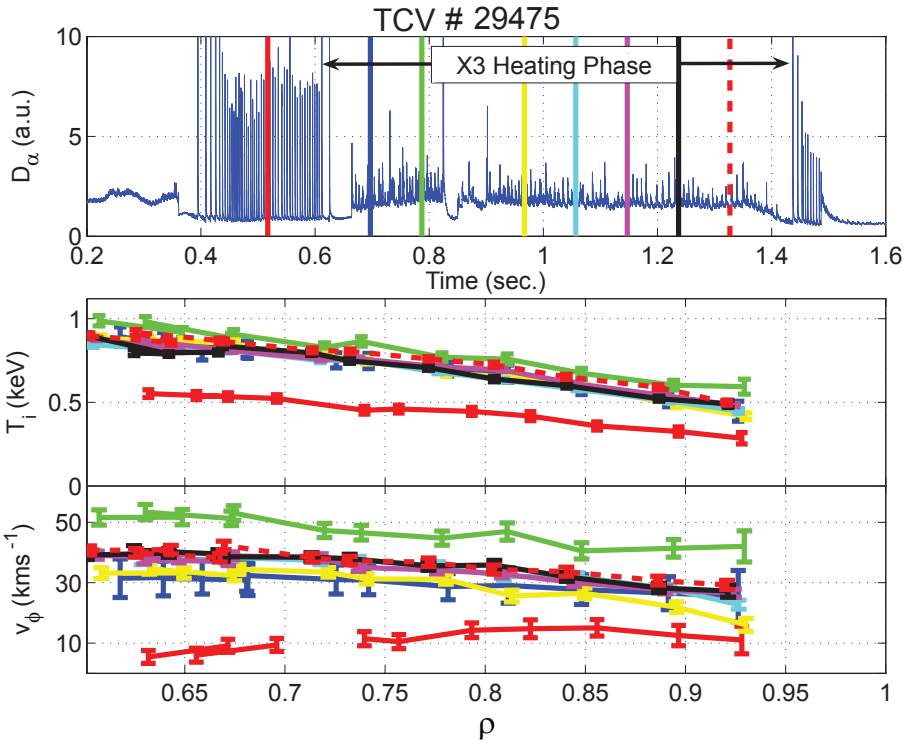

Figure 8. During the ELM-free quasi-stationary H-modes the carbon ion temperature, at $\rho \approx 0.6$ in this case, increased from $\approx 500\ eV$ to $\approx 1\ keV$. At the same time the carbon ion toroidal rotation, at the same location, increase from $\approx 5\ kms^{-1}$ to $\approx 50\ kms^{-1}$. The radial gradient of the toroidal velocity is very small during the QSEFHM phase.

again dominated by m/n = 1/1 modes and both the T_C and $v_{tor,C}$ partially recovered.

In Figure 8 are plotted ion rotation velocity profiles at various times during TCV shot 29475. In the ohmic phase the toroidal rotation velocity was $\approx 10\ kms^{-1}$ and increased to $\approx 50\ kms^{-1}$ in the QSEFHM phase. The rotation velocity was in the co-current direction during both phases. Significantly the radial gradient of the toroidal velocity, inside a normalised radius of 0.93, was almost negligible during the QSEFHM. Even in the ohmic H-mode phase it was small.

4.3.4. Discussion For the first time high power high harmonic electron cyclotron resonance heating has been demonstrated on a high density target H-mode target using vertical launch geometry. The coupled X3 power was much larger than the ohmic power and refraction could be compensated by adjustment of the launch mirror angle a priori. The first pass absorption was in excess of 70% and could be sustained in spite of large plasma perturbations caused by ELMs. In addition the X3 coupled power was the dominant source of heat in these discharges; $P_{X3} > 3.5 \times P_\Omega$. This is a significant result because it shows, for the first time, the feasibility of using vertical launch, high harmonic ECRH in conditions that are fusion relevant.

Ion heating, due to ion-electron collisions, was observed in the QSEFHM phase of X3 heated H-modes. Previous tokamak experiments where H-mode has been achieved and maintained using ECRH [22, 23, 25], have been limited to low density operation, due to the density cut-off, and no effect on the ion temperature was reported. The duration of the H-mode was also limited by the rate of rise of the electron density and the consequent appearance of cut-off; the H-modes were ELM-free and there was, therefore, no density control. Fielding et al [24] reported operation using fundamental ordinary mode ECRH to achieve and maintain H-mode on COMPASS. They obtained relatively poor energy confinement and did not report ion heating. This contrasts with the QSEFHM where ion heating has been observed with high energy confinement.

The QSEFHM is unique and significant. It is unique because it is obtained using pure electron heating with no momentum input. It is significant because ELM mitigation and/or avoidance is an issue crucial to ITER operation. The QSEFHM was achieved in a target plasma that was fusion relevant; $\beta_N \approx 2$ and $\nu_{eff} \approx 0.4$ and $q_{95} = 2.5$ which are values expected for ITER operation.

The QSEFHM is unique but there are, however, several other high confinement modes that are similar in character; high energy confinement, quasi-stationary density, ELM-free.

The Quiescent H-mode first observed on DIII-D [26], but observed also on JET [27] and ASDEX [28] exhibits high energy confinement and moderate particle confinement. This mode requires cryo-pumping, counter-current neutral beam injection and a large plasma to outer wall separation. The density is controlled by an edge plasma oscillation, the Edge Harmonic Oscillation (EHO). A similar mode has not been observed on TCV to date. The QSEFHM is clearly quite different from the quiescent H-mode. One advantage the QSEFHM has over the quiescent H-mode is that it does not rely on NBI heating; an encouraging result in light of the difficulty of producing negative ion sources for NBI heating of next step devices.

On ALCATOR C-MOD the EDA H-mode [29] exhibits high energy confinement and high levels of recycling light as does the TCV quasi-stationary ELM-free H-mode. However, the EDA H-mode is generally obtained at $q_{95} > 3.7$ while on TCV the QSEFHM is obtained at $q_{95} \approx 2.5$. Also, the EDA H-mode is accompanied by broad-band and coherent fluctuations ($f_{fluc} \approx 100\ kHz$) in the edge density and poloidal magnetic field that are believed to moderate the core plasma density. No such high frequency oscillation is observed on TCV.

Both the Type-II ELMy H-mode [30, 31] and the RI-Mode found on TEXTOR [32], which exhibit high confinement and are ELM-free, show little resemblance to the QSEFHM of TCV. They both appear at $n_{e,o}/n_G > 0.8$ and at $\nu_{eff} > 1$.

It is not known what controls the density in the QSEFHM. Despite the fact that no coherent mode, analagous to the EHO, has been observed its existence on TCV cannot be excluded. No edge reflectometry or scattering diagnostics were installed on TCV, for these experiments, so edge density fluctuations could not be measured.

The peaked nature of the density profiles in the X3 heated H-modes is contrary

to predictions of neoclassical transport [33] and as discussed in detail in [34] and [35] may indicate that density profile flattening in ITER under conditions of dominant alpha heating may be less pronounced than feared.

The spontaneous production of toroidal velocity that is observed in the QSEFHM is similar to observations made on other devices. On COMPASS [36], for example, the toroidal velocity increases from $-10\ kms^{-1}$ to $18\ kms^{-1}$ at the L- to H-mode transition. Similar results are reported in the ALCATOR C-MOD tokamak [37]. On TCV the toroidal velocity is typically counter current in L-mode and becomes co-current in ohmic H-mode. The dramatic increase at the onset of the QSEFHM and the small, if not negligible radial gradient of toroidal velocity, both imply that a neoclassical momentum pinch may dominate radial momentum transport [38, 39]. The gradient in momentum density is caused by the density gradient and not the velocity [40]. The temporal resolution of the CXRS diagnostic did not allow detailed measurements of the temporal evolution of the increase in toroidal velocity at the onset of the QSEFHM. Momentum diffusivity of order $0.1\ m^2s^{-1}$ has been reported [41] on ALCATOR C-MOD. A more detailed analysis of momentum transport in the QSEFHM will be presented in a later paper.

5. Conclusions

Using X2 in ECCD and ECRH and X3 in ECRH it has been possible to experimentally examine the dynamics of suprathermal electrons. Fast electron dynamics studies have concentrated on their transport and their effect on the absorption of X3 radiation. Fast electron diffusivity has been estimated to be high but further modelling work is required to verify this. Enhanced X3 bulk electron heating has been measured in the presence of a suprathermal electron population produced by the X3 wave itself. Much work has yet to be done to reconcile the experimental observations on the suprathermal electron dynamics with Fokker-Planck simulations.

Using X3 to heat ELMy H-mode plasma has proven to be a remarkable success. It has been possible to couple up to 85% of launched X3 power to an H-mode target and in so doing substantially alter the plasma dynamics. The X3 power remained well coupled to the plasma even in the presence of large ELMs. This is an encouraging result for the future application of ECRH to next step devices.

For the first time significant collisional ion-heating has been observed in H-mode heated purely by ECRH.

A quasi-stationary ELM-free H-mode that has good energy confinement has been found. It is similar in character to the quiescent H-mode but is believed to be unique in that it requires no neutral beam injection and requires no cryo-pumping. The QSEFHM has some very interesting characteristics, such as its peaked density profiles and high spontaneously produced toroidal momentum, that will be studied in detail in future experimental campaigns.

Acknowledgments

The authors are indebted to the whole TCV team for making this work possible. This work was partly funded by the Fonds National Suisse de la Recherche Scientifique.

References

[1] T.P. Goodman et al, *Nucl Fusion* **43** (2003) 1619-1631
[2] P. Blanchard et al, *Plasma Phys. Control. Fusion* **44** (2002) 2231-2249
[3] S. Coda et al, *Nucl. Fusion* **43** (2003) 1361-1370
[4] S. Alberti et al, *Nucl. Fusion* **42** (2002) 42-45
[5] G. Arnoux at al, *Plasma Phys. Control. Fusion* **47** (2005) 295-314
[6] S. Alberti et al, *Nucl. Fusion* **45** (2005) 1224-1231
[7] I. Klimanov, Thèse No. 3342(2005) École Polytechnique Fédérale de Lausanne
[8] S. Coda et al, *Proc.* 30^{th} *EPS Conf. on Control Fusion and Plasma Physics*, St. Petersburg , Russia, Europhys. Conf. Abstr. 27A (2003) P-3.134
[9] S. Coda et al, *Plasma Phys. Control. Fusion* **48** (2006) B359
[10] L. Porte et al, *Proc.* 20^{th} *IAEA Conference on Fusion and Energy*, Lyon, France (2002)
[11] S. Coda et al, *Phys. Plasmas* **12**, 056124 (2005)
[12] T.P. Goodman et al, *Fusion Technology: Proc.* 19^{th} *Symp. on Fusion Technology*, Lisbon (1996) vol. 1, 565
[13] J-P Hogge et al, *Nucl. Fusion* **43** (2003) 1353-1360
[14] ITER Physics Expert Groups on Confinement and Modelling, *Nucl. Fusion* **29** 12 1999
[15] G. Arnoux, Thèse No. 3401(2005) École Polytechnique Fédérale de Lausanne
[16] K. Matsuda, *IEEE Trans. Plasma Sci.* **17** (1989) 6-11
[17] A. Manini et al, *Plasma Phys. Control. Fusion* **44** (2002) 139-157
[18] B. LaBombard 2001, Plasma Science and Fusion Center, Massachusetts Institute of Technology Report PSFC/RR-01-3
[19] A. Zabolotsky et al 2006 *Plasma Phys. Control. Fusion* **45** 745-746
[20] H. Weisen et al 2006 *Plasma Phys. Control. Fusion* **48** A457-A466
[21] A.N. Karpushov et al, *Fusion Eng. and Design***66-68** (2003) 899-904
[22] J. Lohr et al, *Phys. Rev. Lett.* **60** (1988) 2630-2634
[23] S.J. Fielding et al, *Plasma Phys. Control. Fusion* **28** (1996) 1091-1102
[24] S.J. Fielding et al, *Plasma Phys. Control. Fusion* **40** (1998) 731-735
[25] K. Hoshino et al, *Phys. Rev. Lett.* **63** (1989) 770-774
[26] K. Burrell et al, *Plasma Phys. Control. Fusion* **44** (2002) A253-A263
[27] W. Suttrop et al, *Plasma Phys. Control. Fusion* **45** (2003) 1399-1416
[28] W. Suttrop et al, *Nucl. Fusion* **45** (2005) 721-730
[29] M. Greenwald et al, *Plasma Phys. Control. Fusion* **42** (2000) A263-A269
[30] J. Stober et al, *Nucl. Fusion* **41** (2001) 1123-1134
[31] Y. Kamada et al, *Plasma Phys. Control. Fusion* **42** (200) A247-A253
[32] A.M. Messiaen et al, *Nucl. Fusion* **34** (1994) 825-836
[33] X. Garbet et al, *Plasma Phys. Control. Fusion* **46** (2004) B557-B574
[34] A. Zabolotsky et al, this conference paper EX\P3-7
[35] H. Weisen et al, this conference paper EX\8-4
[36] I.H. Coffey et al, in *Proceedings of the* 11^{th} *Colloquium on UV and X-ray Spectroscopy of Astrophysical and Laboratory Plasmas, Nagoya, Japan 1996*, Frontiers Science Series No. 15, edited by K. Yamashita and T. Watanabe (Universal Academy Press, Tokyo, Japan, 1996) p.431
[37] J.E. Rice et al, *Nucl. Fusion* **37** (1999) 421-426
[38] H. Sugama et al, *Phys. Plasmas* **4** (1997) 2215-228

[39] K. Nagashima et al, *Nucl. Fusion* **34** 449-454
[40] I.H. Hutchinson et al, *Phys. Rev. Lett.* **84** (2000) 3330-3334
[41] J.E. Rice et al, *Phys. Plasmas* **11** (2004) 2427-2432